Distribution of Forces Between Synergistics and Antagonistics Muscles Using an Optimization Criterion Depending on Muscle Contraction Behaviour

Carlos Rengifo*, Yannick Aoustin, Franck Plestan, Christine Chevallereau

Institut de Recherche en Communications et Cybernétique de Nantes
UMR 6597, Ecole Centrale de Nantes, Université de Nantes
1 de la Noë, 44321 Nantes, France

Abstract

In this paper a new neuromusculoskeletal simulation strategy is proposed. It is based on a cascade control approach with an inner muscular-force control loop and an outer joint-position control loop. The originality of the work is located in the optimization criterion used to distribute forces between synergistic and antagonistic muscles. The cost function and the inequality constraints depend on an estimation of the muscle fiber length and its time derivative. The advantages of a such criterion are exposed by theoretical analysis and numerical tests. The simulation model used in the numerical tests consists in an anthropomorphic arm model composed by two joints and six muscles. Each muscle is modeled as a second order dynamical system including activation and contraction dynamics. Contraction dynamics is represented using a classical Hill's model.

*Corresponding author: Address: Institut de Recherche en Communications et Cybernétique de Nantes (IRCCyN), UMR 6597, Ecole Centrale de Nantes, 1 Rue de la Noë BP 92 101,, 44321 Nantes CEDEX 03, France; phone: 33-2-40-37-69-20; fax: 33-2-40-37-69-30; email:Carlos.Rengifo@irccyn.ec-nantes.fr

1 Introduction

Computer simulation has become a very useful tool to investigate how the neuromusculoskeletal system interacts to produce coordinated motions [1]. Neuromusculoskeletal simulation (NS) provides possibilities which are not generally possible by experimental ways. For example, simulations allow to estimate physical variables which cannot be directly measured, or to evaluate the outcome of physically activities which could be dangerous or impossible to do through experimental ways [2], [3], [4]. NS has been also extensively used to study normal and pathological gaits [5], [6], [7], [8], to investigate the transition between walking and running [9], [10]. Even functional electrical stimulation strategies have been tested in simulation before clinical experiments using NS [11].

One of the main difficulties in NS comes from the redundant nature of the biomechanical systems. Redundancy in this context means that the number of muscles is greater than the number of degrees of freedom related to joints. A first way for NS is based on inverse dynamic approaches. Kinematic data are used to estimate joint torques by using inverse dynamic algorithms. Due to the redundancy, the determination of muscular efforts given the joint torques is an indeterminate problem. Several optimization criteria have been proposed to overcome this problem: the minimum sum of muscle efforts [12], the minimum sum of muscle stresses [13] and the minimization of muscular energy consumption [14]. Although, inverse dynamics approach is a computationally efficient technique because it does not involve muscular models. By consequence maximal and minimal muscular forces, which define the inequality constraints of the optimization problem, must be considered as constants. This latter point appears as a main drawback given that these forces strongly depend on

muscular fiber length and its time derivative [15].

A second way for NS uses forward dynamics approaches. It consists in finding a set of muscle excitations, which produce desired motions when applied to forward dynamics equations. However, due to the redundancy, different solutions of excitation patterns produce the same motion. In [16], muscle excitations were taken as the optimization variables, which minimize the metabolic energy consumption. Unfortunately, this approach is computationally expensive: for example, muscle excitations computations for a 3D human walking model require more than 10000 hours of computation with a supercomputer [16]. Another way to overcome redundancy in forward dynamics NS consists in using real electromyographic signals (EMG) [17], [18], [19]. The main difficult of this technique is the estimation of the muscular activations from EMG recordings which requires a complex signal processing [20]. Due to the open loop nature of this technique, the calculated excitation inputs could lead to motions which can be very sensitive to model uncertainties. In our opinion this fact seriously limits its applicability to human walking simulations where stability is a fundamental issue. Another kind of forward NS techniques is based on closed-loop control strategies [21], [22], [23]. The controller inputs are the position and velocity tracking errors with respect to the desired joint trajectories, whereas the outputs are the muscle excitations. As stated in [23], the benefit of this tracking formulation is to constraint the model to produce more realistic behaviors. In other cases, like in human gait simulations, feedback is required to ensure stability. In the aforementioned cases it is assumed that the central nervous system (CNS) defines the muscular excitation patterns as efficiently as possible. For example, in [21] and [22], the Euclidean norm of the steady state muscular activation vector is minimized. This means, the coactivation coefficient is zeroed. Actually, as commonly observed in EMG signals

recordings, it is not the case because synergistic and antagonistic muscles can be activated in the same time.

Optimization methods based on the minimal muscle force, the minimal muscle stress or the minimal energy consumption do not predict co-contraction adequately [24], [25]. Moreover, in most works the solution of the redundancy problem predicts co-contraction only if the model includes joints with multiple degrees of freedom [26] or bi-articular muscles [27]. However, this is not co-contraction in the strict sense of the term [25]. In [28], a shift parameter is introduced in the optimization criterion allowing to obtain co-contraction even for systems with only one degree of freedom. Unfortunately, in the optimization problem, the incidence of the muscle fiber length and its time derivative on the maximal and minimal forces produced by the muscle was not taken into account.

In the current paper, a new neuromusculoskeletal simulation strategy is proposed. Like [21] [22], and [23], a closed-loop control approach is used. An inner loop controls the muscular force and an outer loop tracks the desired motion. The originality of the work is located in the optimization criterion used to distribute forces between synergistic and antagonistic muscles and in the definition of the inequality constraints. This distribution is traditionally made using only the joint torques and the matrix of moments arms. Here, the maximal and minimal musculotendon forces, defining the inequality constraints of the optimization problem, are computed by using an estimation of the muscle fiber length and its time derivative. Using a model of an anthropomorphic arm, it is shown that, when these variables are not included in the optimization problem, the distribution of forces can be unfeasible.

The document is organized as follows. In Section 2, the maximal and the minimal forces of a second-order musculotendon dynamic model are computed as a function of muscular

fiber length and its time derivative. In Section 3, the model of an anthropomorphic arm composed of two joints and six muscles is presented. This model is used to test the proposed musculoskeletal simulation strategy. Section 4 is devoted to the main contribution of this paper: the force sharing problem between synergistic and antagonistic muscles is addressed. Numerical tests comparing the new optimization criterion with the criterion proposed in [28] are presented in Section 5. The last Section offers our conclusions and perspectives.

2 Musculotendon model

Many muscle models can be found in the literature, ranging from very simple [29] to highly complex [30] ones. On biomechanical applications the most popular models are based on the phenomenological mechanical representation proposed by Hill in [31]. A modification of the previous models including fatigue/recovery effects is presented in [32]. The current one uses the Hill's mechanical model completed by Zajac [15] by defining the connection between the excitation and activation signals. As displayed in Figure 1, a musculotendon unit is composed by activation and contraction dynamics. The inputs are the muscle excitation u, and the musculotendon fiber length $l_{mt}(q)$ which depends on the joint positions q relative to the skeletal model. The output f_t is the force developed by the tendon whereas a is the muscle activation level. In the model proposed in [15], four parameters and four curves are required to describe the contraction dynamics. The parameters are the maximum isometric force f_o, the optimal fiber length l_{o}, the tendon slack length l_s and the pinnation angle between the fibers of the tendon and the fibers of the muscle. The latter has been supposed equal to zero without loss of generality for our consideration. The tendon model is based

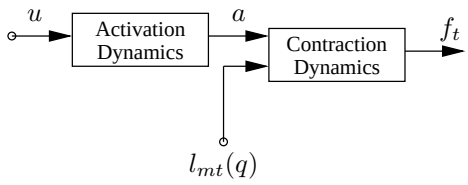

Figure 1: Scheme of a musculotendon unit.

on a function f_t describing the force-length relationship whereas the muscle model requires the passive force f_p and the active force f_a. The last one is defined as the product of three tems: the muscular activation a, and the force-length and the force-velocity relationships, respectively noted f_l and f_v ($f_a = a \cdot f_l \cdot f_v$).

2.1 Activation dynamics

Activation dynamics establish the relationship between the muscular excitation u and the mechanical activation a. A bilinear activation model is presented in [15]. However in the sake of simplicity, the piecewise linear model model proposed in [33] has been used

$$\dot{a} = \begin{cases} -\dfrac{a}{\tau_a} + \dfrac{u}{\tau_a}, & u \geq a \\ \\ -\dfrac{a}{\tau_d} + \dfrac{u}{\tau_d}, & u < a \end{cases} \tag{1}$$

τ_a and τ_d being respectively the activation and deactivation time constants. Excitation and activation levels are allowed to continuously vary between 0 and 1 [15].

2.2 Contraction dynamics

As displayed in Figure 2, the contraction dynamics is represented as a mechanical system composed by the models of both tendon and muscle [15]. The muscle is composed by two

elements which are passive and active respectively (Figure 2). The muscular force is the sum of f_p, the force generated by the passive element, and f_a, the force generated by the active element. From data of [15] we have approximated functions f_p, f_l and f_v by tangent sigmoid functions because they are continuous and derivable in the scale of study and offer an accurate representation. Other aproximations for these functions have been proposed in [33].

Tendon force: The tendon is considered as a passive element which yields

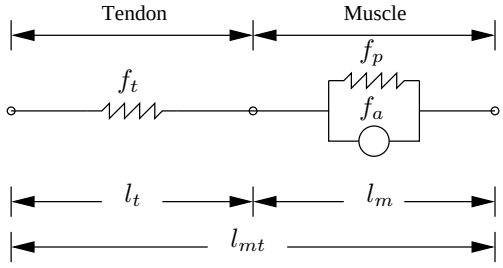

Figure 2: Hill-type model of a musculotendon unit [15].

$$f_t\left(l_t\right) = K_t\left[\frac{l_t - l_s}{l_s}\right] \cdot f_o \tag{2}$$

with f_t the tendon force, l_t the tendon length, l_s the tendon slack length, K_t the tendon stress-strain constant and f_{o} the maximum isometric force. l_t is supposed ranging from l_s to $1.1 \cdot l_s$. The value $l_t = 1.1 \cdot l_s$ is the maximal tendon length before rupture [15].

Muscular passive force: The force f_p is modeled by the equation

$$f_p\left(\bar{l}_m\right) = \frac{2.5}{1 + e^{-12\left(\bar{l}_m - 1.425\right)}} \cdot f_{\mathrm{o}}$$

with $\bar{l}_m \equiv l_m / l_{\mathrm{o}}$ the normalized muscle length, l_{o} the optimal fiber length and f_{o} the maximum isometric force. The muscle length l_m is supposed ranging from $0.5 \cdot l_{\mathrm{o}}$ to $1.8 \cdot l_{\mathrm{o}}$ [15].

Muscular Active force: The active element represents the muscle ability to generate force as a function of the muscular activation a. The active force f_a is the product of four terms: the length-force relation $f_l\left(\bar{l}_m\right)$, the velocity-force relation $f_v\left(\dot{\bar{l}}_m\right)$ the muscular activation level a and the maximum isometric force f_{o}

$$f_a\left(a, \bar{l}_m, \dot{\bar{l}}_m\right) = a \cdot f_l\left(\bar{l}_m\right) \cdot f_v\left(\dot{\bar{l}}_m\right) \cdot f_{\mathrm{o}} \tag{3}$$

Functions $f_l(.)$ and $f_v(.)$ depicted in Figure 3 read as:

- Length-force relation

$$f_l\left(\bar{l}_m\right) = \left[\frac{1}{1+e^{-12\left(\bar{l}_m-0.6\right)}} + \frac{1}{1+e^{+12\left(\bar{l}_m-1.4\right)}} - 1\right] \tag{4}$$

- Force-velocity relation

$$f_v\left(\dot{\bar{l}}_m\right) = \begin{cases} f_{v_{\min}}, & \dot{\bar{l}}_m < \dot{\bar{l}}_{m_{\min}} \\ \dfrac{2}{1+e^{-6\dot{\bar{l}}_m}}, & \dot{\bar{l}}_{m_{\min}} \leq \dot{\bar{l}}_m \leq \dot{\bar{l}}_{m_{\max}} \\ f_{v_{\max}}, & \dot{\bar{l}}_m > \dot{\bar{l}}_{m_{\max}} \end{cases} \tag{5}$$

with

$$\dot{\bar{l}}_{m_{\min}} = -1 \qquad f_{v_{\min}} = \frac{2}{1+e^6}$$
$$\dot{\bar{l}}_{m_{\max}} = -\frac{1}{6}\ln\left(\frac{2}{1.8} - 1\right) \qquad f_{v_{\max}} = 1.8$$

The parameters $\dot{\bar{l}}_{m_{\min}}$ and $f_{v_{\max}}$ are taken from [15], $\dot{\bar{l}}_{m_{\max}}$ and $f_{v_{\min}}$, are deduced in order to guarantee the continuity of f_v with respect to $\dot{\bar{l}}_m$.

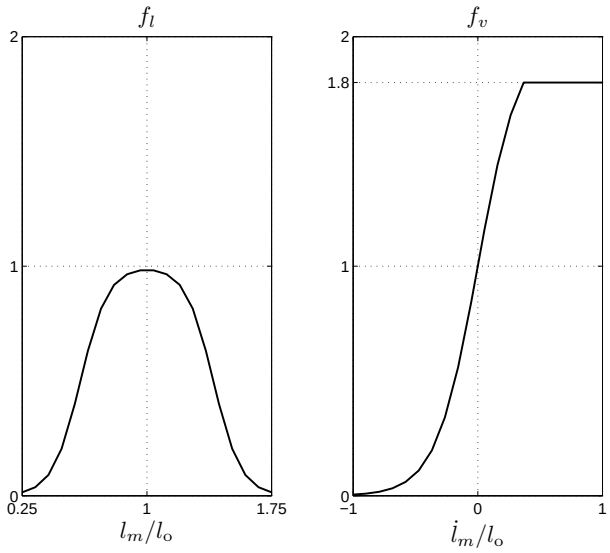

Figure 3: **Active force:** The force-length and force-velocity relationships.

Fiber length dynamics: Forces f_t, f_p, and f_a acting on the musculotendon unit (Figure 2) yield to an equilibrium such that

$$\begin{aligned} f_t\left(l_t\right) &= f_p\left(\bar{l}_m\right) + f_a\left(a, \bar{l}_m, \dot{\bar{l}}_m\right) \\ &= f_p\left(\bar{l}_m\right) + a \cdot f_l\left(\bar{l}_m\right) \cdot f_v\left(\dot{\bar{l}}_m\right) \cdot f_o \end{aligned} \tag{6}$$

Given $l_t = l_{mt} - l_m$ (see Figure 2), one gets

$$f_t\left(l_{mt} - \bar{l}_m \cdot l_o\right) = f_p\left(\bar{l}_m\right) + a \cdot f_l\left(\bar{l}_m\right) \cdot f_v\left(\dot{\bar{l}}_m\right) \cdot f_o \tag{7}$$

Recalling that a and l_{mt} are the inputs of the contraction dynamics model (Figure 1), the contraction dynamics is given through the inversion of the function f_v (from (5))

$$\dot{\bar{l}}_m = g_{cd}\left(f_v\right) \equiv \begin{cases} \dot{\bar{l}}_{m_{\min}}, & f_v < f_{v_{\min}} \\ -\dfrac{1}{6}\ln\left(\dfrac{2}{f_v} - 1\right), & f_{v_{\min}} \leq f_v \leq f_{v_{\max}} \\ \dot{\bar{l}}_{m_{\max}}, & f_v > f_{v_{\max}} \end{cases} \tag{8}$$

The argument f_v of the above equation is deduced from (7)

$$f_v = \frac{f_t\left(l_{mt} - \bar{l}_m \cdot l_{\mathrm{o}}\right) - f_p\left(\bar{l}_m\right)}{a \cdot f_l\left(\bar{l}_m\right) \cdot f_{\mathrm{o}}} \tag{9}$$

When $f_v \in [f_{v_{\min}}, f_{v_{\max}}]$, $\dot{\bar{l}}_m$ lies in the interval $[\dot{\bar{l}}_{m_{\min}}, \dot{\bar{l}}_{m_{\max}}]$. Indertemination and division by zero are prevented by restricting the minimal value of a to 10^{-6}. As f_v depends on the variables $\bar{l}_m$, a and l_{mt}, one gets

$$\dot{\bar{l}}_m = g_{cd}\left(\bar{l}_m, a, l_{mt}\right) \tag{10}$$

The output of the musculotendon unit is the tendon force. It can obtained by rewriting (2) in terms of $\bar{l}_m$ and the input l_{mt}

$$f_t = K_t\left[\frac{l_{mt} - \bar{l}_m \cdot l_{\mathrm{o}} - l_s}{l_s}\right] \cdot f_{\mathrm{o}} \tag{11}$$

A block diagram representing the contraction dynamics is presented in Figure 4.

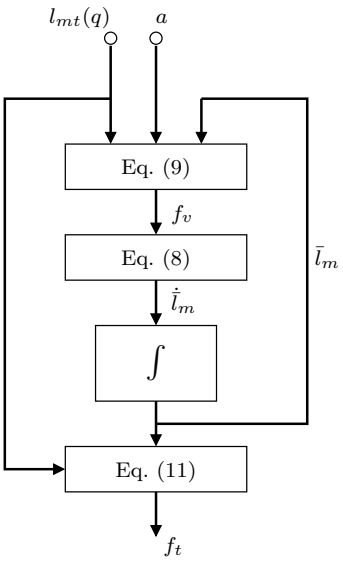

Figure 4: **Contraction dynamics:** The output of the model is the musculotendon force f_t and the external inputs are the activation level a and the musculotendon length l_{mt}.

2.3 Maximal and minimal musculotendon forces

For a given $\bar{l}_m$ and $\dot{\bar{l}}_m$, the maximal and minimal musculotendon forces can be respectively computed evaluating the equation (7) at $a_{\min} = 10^{-6}$ and $a_{\max} = 1$

$$\begin{aligned} f_{t_{\min}} &= f_p\left(\bar{l}_m\right) + a_{\min} \cdot f_l\left(\bar{l}_m\right) \cdot f_v\left(\dot{\bar{l}}_m\right) \cdot f_o \\ f_{t_{\max}} &= f_p\left(\bar{l}_m\right) + a_{\max} \cdot f_l\left(\bar{l}_m\right) \cdot f_v\left(\dot{\bar{l}}_m\right) \cdot f_o \end{aligned} \tag{12}$$

When $\dot{\bar{l}}_m$ tends to its minimal value f_v tends to zero (Figure 3) and by consequence the maximal and minimal forces becomes equals to $f_p\left(\bar{l}_m\right)$. In such case, the force of the musculotendon unit cannot be freely imposed, it is uniquely determined by the muscular fiber length. As it can be seen from Figure 5, the minimal achievable musculotendon force is not always zero, it strongly depends on the muscular fiber length.

In Figure 6, the maximal musculotendon force is plotted as a function of $\bar{l}_m$ and $\dot{\bar{l}}_m$. These fig-

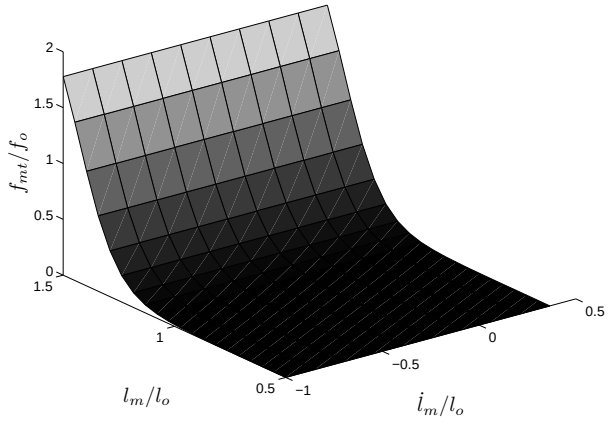

Figure 5: **Minimal normalized musculotendon force:** It is obtained when the muscular activation is at its minimal value ($a = 10^{-6}$).

ures show that the upper and lower limits on the forces exerted by a muscle are not constant. There are functions of $\bar{l}_m$ and $\dot{\bar{l}}_m$. These non constant constraints must be considered in the optimization problem solved to distribute the forces between synergistics and antagonistics muscles.

3 Anthropomorphic arm model

The anthropomorphic arm is depicted in Figure 7. The arm model is composed of 6 muscles and 2 joints representing the shoulder and the elbow. The anthropomorphic arm is considered evolving in a vertical plane. The inputs are the muscular excitations and the outputs are joints positions. The inputs u_i ($i = \{1 \dots 6\}$) directly define muscular activations a_i ($i = \{1 \dots 6\}$) through activation dynamics (1). The musculotendon lengths $L_{mt} = [l_{mt_1} \cdots l_{mt_6}]^T$ and the muscular activations are used by the contraction dynamics to obtain the musculotendon forces f_{t_i} ($i = \{1 \dots 6\}$). The joint torques Γ_i ($i = \{1, 2\}$) are

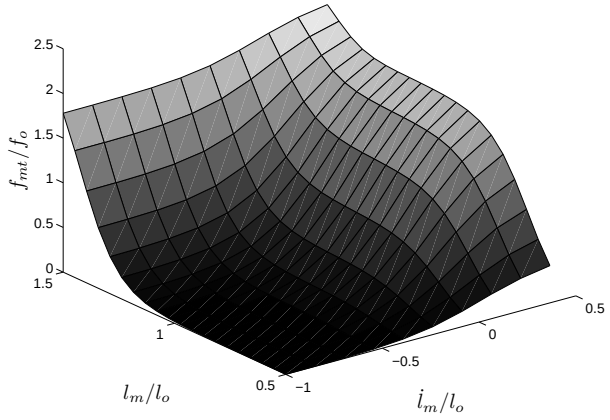

Figure 6: **Maximal normalized musculotendon force:** It is obtained when the muscular activation is at its maximal value ($a = 1$).

computed as the product of the musculotendon forces by the matrix of moment arms. The torques are the inputs to the skeletal dynamics, which is used to determine joint positions and velocities. The musculotendon lengths mentioned above are given by the musculo-skeletal geometry as a function of the joint positions. A block diagram describing the interaction between the subsystems composing the arm model is presented in Figure 8.

3.1 Skeletal dynamics

The relationship between torques and joint accelerations are given by the skeletal dynamics

$$D\left(q_2\right)\ddot{q} + C\left(q, \dot{q}\right)\dot{q} + G(q) = \Gamma \tag{13}$$

with $q = \begin{bmatrix} q_1 & q_2 \end{bmatrix}^T$ respectively representing the shoulder and elbow joint angles[1], $D(q_2)(2 \times 2)$ the symmetric positive inertia matrix, $C(q, \dot{q})(2 \times 2)$ the Coriolis and centrifugal effects

[1]Notation ^{T} denotes matrix transposition.

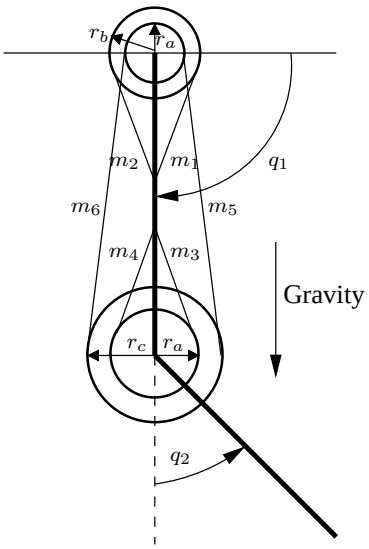

Figure 7: **Schematic representation of the anthropomorphic arm**. The arm motion is made by 6 muscles: 4 monoarticular ones (m_1, m_2, m_3, m_4) and 2 biarticular ones (m_5,m_6).

matrix and $G(q)(2 \times 1)$ the gravity effects vector. The vector $\Gamma = \begin{bmatrix} \Gamma_1 & \Gamma_2 \end{bmatrix}^T$ is composed by the torques applied at each joint. Arm parameters are displayed in Table 1.

3.2 Activation and contraction models

For each muscle activation and contraction models are based on the equations (1) and (10). Let us to note u_i, a_i, l_{mt_i}, $\bar{l}_{m_i}$, f_{t_i} as the muscular excitacion, the muscular activation, the musculotendon fiber length, the normalized muscular fiber length and the tendon force of the muscle i ($i = 1 \ldots 6$). The parameters for each muscle are given in Table 2

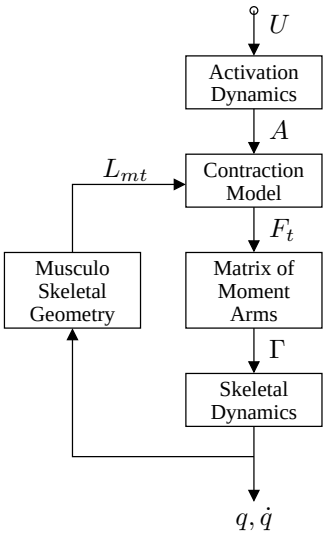

Figure 8: **Anthropomorphic arm block diagram**. $U = [u_1 \cdots u_6]^T$ is the muscular excitations vector (and then the control input vector). $A = [a_1 \cdots a_6]^T$ is the muscular activations vector. $F_t = [F_{t_1} \cdots F_{t_6}]^T$ is the musculotendon forces vector. $L_{mt} = [l_{mt_1} \cdots l_{mt_6}]^T$ is the musculotendon fiber length vector. $\Gamma = [\Gamma_1 \ \ \Gamma_2]^T$ is the joint torques vector. $q = [q_1 \ \ q_2]^T$ is the joint positions vector.

3.3 Moment arms matrix

As no muscles are directly attached to the second segment (Figure 7), the relationship between torques and forces is given by a constant matrix

$$\begin{bmatrix} \Gamma_1 \\ \\ \Gamma_2 \end{bmatrix} = R \cdot \begin{bmatrix} f_{mt_1} \\ \vdots \\ f_{mt_6} \end{bmatrix} \tag{14}$$

with

$$R = \begin{bmatrix} r_a & -r_a & 0 & 0 & r_b & -r_b \\ 0 & 0 & r_a & -r_a & r_c & -r_c \end{bmatrix}$$

Description	Parameter	Value	Unit
Upper arm mass	M_1	1.8	kg
Forearm mass	M_2	1.6	kg
Upper arm length	l_1	0.32	m
Forearm length	l_2	0.32	m
Upper arm center of mass	c_1	0.16	m
Forearm center of mass	c_2	0.16	m
Inertia of upper arm	I_1	0.015	kg.m^2
Inertia of forearm	I_2	0.013	kg.m^2

Table 1: Skeletal parameters of the anthropomorphic arm model [34].

Parameter	m_1	m_2	m_3	m_4	m_5	m_6	Unit
τ_a	0.04	0.04	0.04	0.04	0.04	0.04	sec
τ_d	0.07	0.07	0.07	0.07	0.07	0.07	sec
f_{o}	2000	2000	900	900	600	600	N
l_s	0.02	0.02	0.02	0.02	0.04	0.04	m
l_{o}	0.11	0.11	0.11	0.11	0.17	0.17	m

Table 2: Muscle parameters of the arm model [34].

with f_{t_i} the force developed by the musculotendon i. The coefficients of the matrix R are given in meters: $r_a = 0.03$, $r_b = 0.025$ and $r_c = 0.04$ [34].

3.4 Musculo-skeletal geometry

Muscles are now attached to both segments of the arm. It means that their lengths depend on the articular positions. Denoting $l^r_{mt_i}$ the rest length of the musculotendon i and q_{r_j} the rest position of joint j, the relation between musculotendon fiber length and joint positions reads as

$$\begin{bmatrix} l_{mt_1} \\ \vdots \\ l_{mt_6} \end{bmatrix} = \begin{bmatrix} l^r_{mt_1} \\ \vdots \\ l^r_{mt_6} \end{bmatrix} - R^T \begin{bmatrix} q_1 - q_{r_1} \\ \\ q_2 - q_{r_2} \end{bmatrix} \tag{15}$$

The shoulder rest angle is $q_{r_1} = -\pi/4$ and the elbow rest angle is $q_{r_2} = \pi/4$.

3.5 Desired motion

The desired motion for the arm is periodic and concerns only the elbow. Without loss of generality the desired position for the shoulder is constant ($q^d_1(t) \equiv 0$). The first half-cycle of the motion begins at $q^d_2(0) = 0$ and finishes at $q^d_2(t_\mathrm{m}) = 5\pi/9$. The second half-cycle begins at $q^d_2(t_\mathrm{m}) = 5\pi/9$ and is ended when $q^d_2(2t_\mathrm{m}) = 0$.

$$q^d_2(t) = \begin{cases} \dfrac{q_f}{t_\mathrm{m}} \left[t - \dfrac{t_\mathrm{m}}{2\pi} \sin\left(\dfrac{2\pi}{t_\mathrm{m}} t \right) \right] & 0 \le t < t_\mathrm{m} \\ \\ q_f - \dfrac{q_f}{t_\mathrm{m}} \left[t - \dfrac{t_\mathrm{m}}{2\pi} \sin\left(\dfrac{2\pi}{t_\mathrm{m}} t \right) \right] & t_\mathrm{m} \le t < 2t_\mathrm{m} \end{cases} \tag{16}$$

with $q_f = 5\pi/9$. For the simulation results presented in Section 5, the parameter t_m has been fixed to 2.5 sec.

4 Kinematic tracking

The proposed forward dynamics closed loop strategy for NS is composed by two control loops. The outer loop uses the kinematic tracking error to compute the desired torques for the two joints. Then, an optimization process is used to define the desired forces for the six inner loops. The primary controller uses a computed torque approach to linearize and to decouple the skeletal dynamics (13)

$$\Gamma^d = D\left(q_2\right)\eta + C\left(q, \dot{q}\right)\dot{q} + G(q) \tag{17}$$

Vector $\eta \in I\!R^2$ is composed by the desired joint accelerations. Each component of η, named η_1 and η_2, is chosen such that

$$\eta_i = \ddot{q}_i^d + k_{p_i}\left(q_i^d - q_i\right) + k_{d_i}\left(\dot{q}_i^d - \dot{q}_i\right), \qquad i = \{1, 2\} \tag{18}$$

q_i^d, $\dot{q}_i^d$ and $\ddot{q}_i^d$ define the desired trajectory for the joint i.

The next step of the proposed musculoskeletal simulation strategy consists in computing the desired forces for the six inner loops. Given Γ_1^d and Γ_2^d, the components of vector Γ^d and the moments arm matrix $R(q)$, the desired musculotendon forces $f_{t_i}^d$ $(i = \{1 \ldots 6\})$ are determined as the solution of the following underdetermined system of linear algebraic equations

$$\begin{bmatrix} \Gamma_1^d \\ \\ \Gamma_2^d \end{bmatrix} = R \cdot \underbrace{\begin{bmatrix} f_{mt_1}^d \\ \\ \vdots \\ \\ f_{mt_6}^d \end{bmatrix}}_{F_{mt}^d} \tag{19}$$

In order to solve the previous system, a standart way consists to minimize the sum of the squared normalized musculotendon forces [35], [36] which yields

$$\begin{aligned} \text{minimize} \quad & \sum_{i=1}^{6} \left(\frac{f_{t_i}^d}{f_{o_i}} \right)^2 \\ \text{subject to} \quad & \Gamma^d = R \cdot F_t^d \\ & f_{t_i}^d \geq 0 \end{aligned} \tag{20}$$

with f_{o_i} the maximum isometric force of the muscle i. At each instant time, the optimization problem (20) must be solved. When criterion (20) is used, co-contraction is possible only if the model includes joints with multiple degrees of freedom [26] or bi-articular muscles [27]. However, this is not co-contraction in the strict sense of the term [25]. A modification of (20) has been proposed in [28] with

$$\begin{aligned} \text{minimize} \quad & \sum_{i=1}^{6} \left(\frac{f_{t_i}^d}{f_{o_i}} - \alpha \right)^2 \\ \text{subject to} \quad & \Gamma^d = R \cdot F_t^d \\ & f_{t_i}^d \geq 0 \end{aligned} \tag{21}$$

For a sake of clarity a simple system will be used to illustrate the effect of the parameter α in the muscular co-contraction.

Example. Consider the following system composed of two antagonist muscles and one joint

$$\Gamma^d = \begin{bmatrix} r & -r \end{bmatrix} \cdot \begin{bmatrix} f_{t_1}^d \\ \\ f_{t_2}^d \end{bmatrix}, \tag{22}$$

with $r > 0$. The objective being to solve the following quadratic optimization problem

$$\begin{aligned} \text{minimize} \quad & \left(\frac{f_{t_1}^d}{f_o} - \alpha\right)^2 + \left(\frac{f_{t_2}^d}{f_o} - \alpha\right)^2 \\ \text{subject to} \quad & \Gamma^d = r \cdot f_{t_1}^d - r \cdot f_{t_2}^d \\ & f_{t_1}^d \geq 0, \quad f_{t_2}^d \geq 0 \end{aligned} \tag{23}$$

The optimal musculotendonforces $f_{t_1}^d$ and $f_{t_2}^d$ are given by

$$f_{t_1}^d = \begin{cases} \alpha f_o + \Gamma^d/2r & \Gamma^d \geq -2\alpha r f_o \\ 0, & \text{otherwise} \end{cases} \tag{24}$$

$$f_{t_2}^d = \begin{cases} \alpha f_o - \Gamma^d/2r & \Gamma^d \leq 2\alpha r f_o \\ 0, & \text{otherwise} \end{cases}$$

When $\alpha = 0$, criterion (23) coincides with criterion (21) and leads to a solution without co-contraction: if the desired torque is negative, $f_{t_1}^d$ is zero. Conversely, when Γ^d is positive, $f_{t_2}^d$ is zero. If Γ^d is zero both forces are zero. When $\alpha > 0$, co-contraction exists only if $\Gamma^d < |2r f_o \alpha|$ otherwise one of the musculotendon forces is zero.

♦

For system (19), the optimization of (20) leads to zero co-contraction when Γ_1^d and Γ_2^d have the same sign. If Γ_1^d and Γ_2^d are greater than zero, then the forces $f_{t_2}^d$, $f_{t_4}^d$ $f_{t_6}^d$, which produce negative torques are zero. Conversely, when Γ_1^d and Γ_2^d are both negatives, then the forces $f_{t_1}^d$, $f_{t_3}^d$ $f_{t_5}^d$, which produce positive torques are zero. These facts can be directly deduced from the moment arms matrix (14). As it was explained in Section 2.2, $f_{t_i}^d$ equal to zero cannot be obtained for some musculotendon lengths (see Figure 5). If Γ_1^d and Γ_2^d have different

signs, co-contraction appears. As it will see in the next section, solutions of the optimization problem (21) with a constant α can produce non-achievable desired musculotendon forces because the maximal and minimal forces which a musculotendon unit can produce are not constant. They strongly depend on l_{m_i} and $\dot{l}_{m_i}$ (Figure 6).

Proposition. Let introduce a parameter α_i for each force $f_{t_i}^d$ as a function of l_{m_i} and $\dot{l}_{m_i}$

$$\begin{aligned} \text{minimize} \quad & \sum_{i=1}^{n} \left[\frac{f_{t_i}^d}{f_{o_i}} - \alpha_i \left(l_{m_i}, \dot{l}_{m_i} \right) \right]^2 \\ \text{subject to} \quad & \Gamma^d = R \cdot F_t^d \\ & f_{\min_i} \leq f_{t_i}^d \leq f_{\max_i} \end{aligned} \tag{25}$$

with

$$\alpha_i \left(l_{m_i}, \dot{l}_{m_i} \right) = \bar{f}_{\min_i} + \frac{\bar{f}_{\max_i} - \bar{f}_{\min_i}}{2} \tag{26}$$

This term is introduced in order to be as far as possible from the limits of the musculotendon forces. The maximal and minimal normalized musculotendon forces are given by (12), which yields

$$\bar{f}_{\min_i} = f_p \left(\bar{l}_{m_i} \right) / f_o + a_{\min} \cdot f_l \left(\bar{l}_{m_i} \right) \cdot f_v \left(\dot{\bar{l}}_{m_i} \right)$$

$$\bar{f}_{\max_i} = f_p \left(\bar{l}_{m_i} \right) / f_o + a_{\max} \cdot f_l \left(\bar{l}_{m_i} \right) \cdot f_v \left(\dot{\bar{l}}_{m_i} \right)$$

The proposed strategy including index (25) is described by Figure 9.

♦

When criterion (25) is used the inequality constraints are often actives. That implies activation levels near to saturation. In order to solve this problem we have introduced the

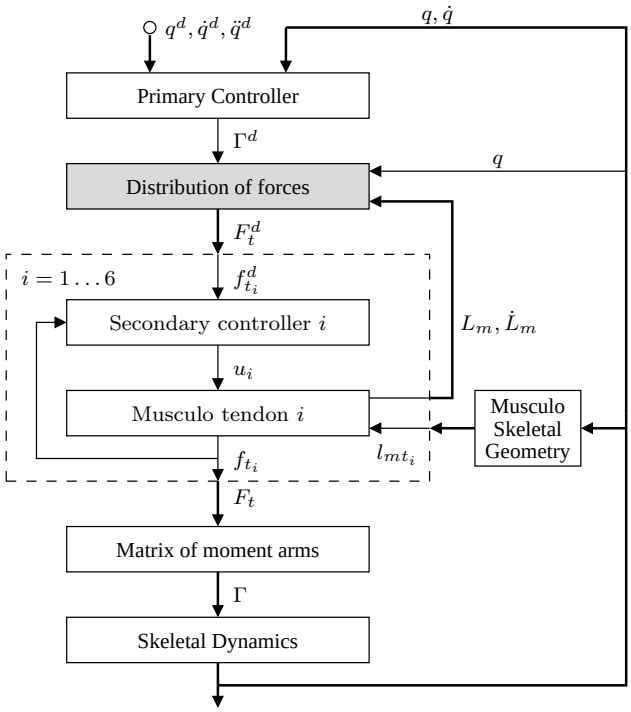

Figure 9: **The proposed musculoskeletal simulation strategy**. $U = [u_1 \cdots u_6]^T$ is the muscular excitations vector (and then the control input vector). $F_t = [F_{t_1} \cdots F_{t_6}]^T$ is the musculotendon forces vector. $L_{mt} = [l_{mt_1} \cdots l_{mt_6}]^T$ is the musculotendon fiber length vector. $\Gamma = [\Gamma_1 \ \Gamma_2]^T$ is the joint torques vector. $q = [q_1 \ q_2]^T$ is the joint positions vector. Γ^d, F_t^d and q^d respectively represent the desired values of the variables Γ, F_t and q.

weighting factor $\omega_i = \left(\bar{f}_{\max_i} - \bar{f}_{\min_i}\right)^{-1}$ in the cost function

$$\begin{aligned} \text{minimize} \quad & \sum_{i=1}^{6} \omega_i \left[\frac{f_{t_i}^d}{f_{o_i}} - \alpha_i \left(l_{m_i}, \dot{l}_{m_i} \right) \right]^2 \\ \text{subject to} \quad & \Gamma^d = R \cdot F_t^d \\ & f_{\min_i} \leq f_{mt_i}^d \leq f_{\max_i} \end{aligned} \tag{27}$$

A feedback linearization control [37] law was used for the inner loop (the so-called secondary controller in Figure 9). The equation giving the musculotendon force (11) is derived with

respect to time in order to involve the muscular activation a

$$\begin{aligned}\dot{f}_t &= \frac{\partial f_t}{\partial l_{mt}} \cdot \dot{l}_{mt} + \frac{\partial f_t}{\partial \bar{l}_m} \cdot \dot{\bar{l}}_m \\ &= \frac{k_t}{l_s} \cdot \dot{l}_{mt} - \frac{k_t \cdot l_o}{l_s} g_{cd}\left(\bar{l}_m, a, l_{mt}\right)\end{aligned}$$

The controller design consists in finding the activation a such that dynamical behaviour of f_t is linear

$$\dot{f}_t = k_f \left(f_t^d - f_t\right)$$

with $k_f = 10$ a constant gain and f_t^d the desired force. When the function g_{cd} reads as the second line of (8) one gets

$$a = \frac{f_t - f_p}{2 f_l} \left[e^{\frac{6 l_s}{k_t \cdot l_o} \left(k_f \left(f_t^d - f_t\right) - \frac{k_t}{l_s} \cdot \dot{l}_{mt} \right)} + 1 \right]$$

which guarantees that equation (4) is fulfilled. The input to the musculotendon unit is the muscular excitation and not the muscular activation. Thus, the controller synthesis is made by assuming no dynamics between the activation and the excitation signals, then the relation between the two variables can be defined by a gain which is equal to 1 according to (1).

5 Numerical tests

The proposed NS strategy of Section 4 has been applied to the anthropomorphic arm described in Section 3. The musculotendon forces presented in Figure 10 are obtained by applying criterion (21) with $\alpha = 1/3$. In this case the musculotendon unit 3 cannot track the desired force in the time interval $[1.3, 2.1]$ (Figure 10). In such interval the desired force is greater than the maximal one. Depending on the values of l_m and $\dot{l}_m$, $\alpha = 1/3$ can be very high (muscle 3 at $1.3 < t < 2.1$ sec) or very low (muscle 4 at $4.2 < t < 5$ sec). The

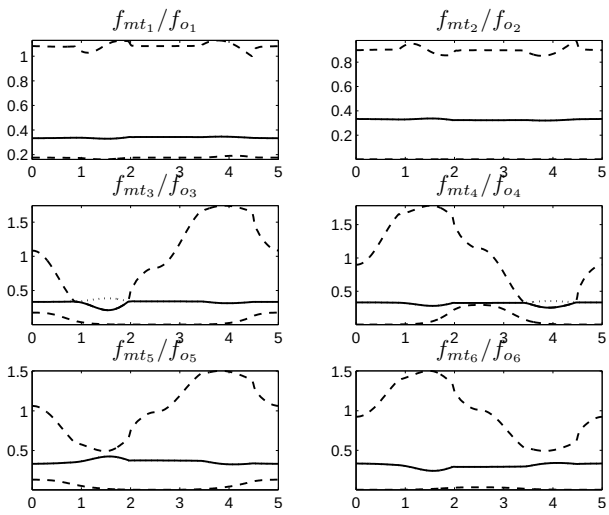

Figure 10: **Distribution of forces using criterion** (21) **($\alpha = 1/3$).** Normalized musculotendon forces versus time. Desired force (dotted line). Musculotendon force (solid line). Maximal and minimal achievable musculotendon forces (dashed lines).

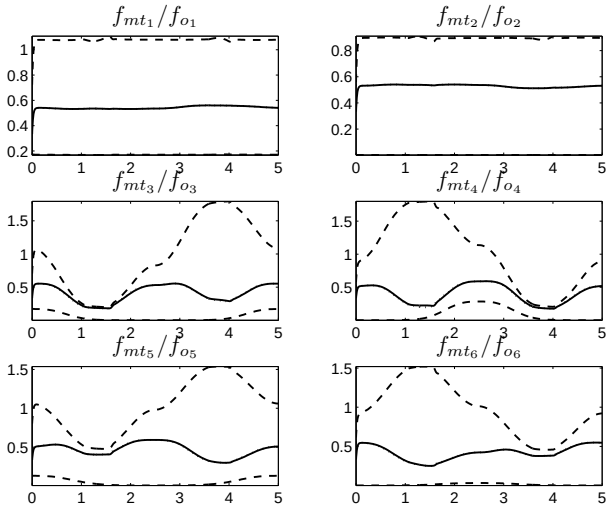

Figure 11: **Distribution of forces using criterion** (27)**.** Normalized musculotendon forces versus time (*sec*). Desired force (dotted line). Musculotendon force (solid line). Maximal and minimal achievable musculotendon forces (dashed lines).

musculotendon forces presented in Figure 11 are obtained by applying criterion (27). For this simulation, the parameter t_{m} has been fixed to 3.0 sec. A comparison between the muscular activations obtained from both criteria (21) and (27) is presented in Figure 12. As it can be seen from this Figure, an optimization criterion independent of maximal and minimal instantaneous forces leads to saturation in the muscular activation even for slow motion. If saturation occurs, the muscular forces cannot track the desired forces, and by consequence a position tracking error appears (Figure 13).

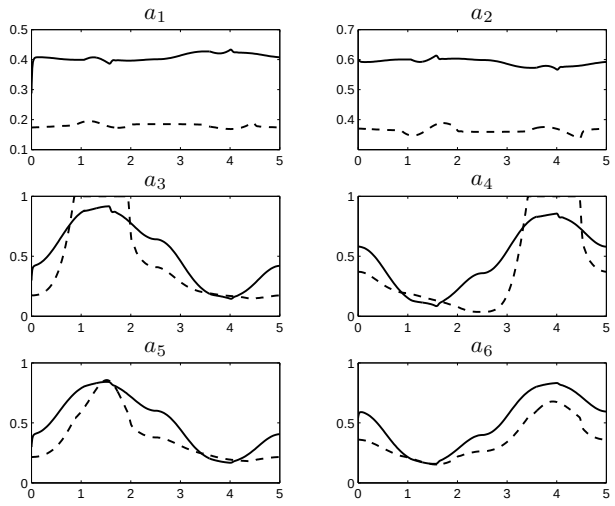

Figure 12: **Muscular activations versus time (*sec*).** Criterion (21) (dashed line). Criterion (27) (solid line)

6 Conclusion and perspectives

An optimization criterion for force sharing between synergistic and antagonistic muscles has been proposed. A cost function depending on muscle fiber length and its derivative appears to crucial in order to avoid saturation in muscle activation levels. If saturation occurs, the

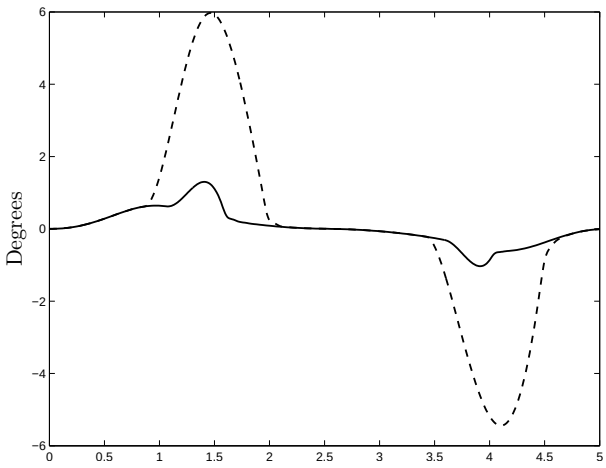

Figure 13: **Elbow position tracking error versus time (*sec*).** Criterion (21) (dashed line). Criterion (27) (solid line).

muscular forces cannot track the desired forces, and by consequence the joint torques are different of the desired ones. In this situation, the musculoskeletal system cannot follow the desired motion.

In systems with one joint, optimization methods depending only on the matrix of moment arms and the torques lead to an increasing or decreasing in unison of the forces in synergistic muscles [38]. However an experimental test shows that it is not necessarily the case [39]. On the other hand, for systems with almost two of joints, like the anthropomorphic arm presented here, these optimization strategies can produce an increase of force in a muscle and a decrease in some of its synergistics. Thus, a further work consists to test our strategy on a biomechanical system with one joint and to verify how the distribution of forces between synergistics muscles is done.

References

[1] Zajac, F. E., 2002, "Understanding muscle coordination of the human leg with dynamical simulations," Journal of Biomechanics, **35**(8), pp. 1011–1018.

[2] Wright, I. C., Neptune, R. R., Van Den Bogert, A. J., and Nigg, B. M., 2000, "The effects of ankle compliance and flexibility on ankle sprains," Medicine & Science in Sports & Exercise, **32**, pp. 260–265.

[3] Wright, I., Neptune, R., van den Bogert, A., and Nigg, B., 2000, "The influence of foot positioning on ankle sprains," Journal of Biomechanics, **33**(5), pp. 513 – 519.

[4] McLean, S. G., Huang, X., Su, A., and van den Bogert, A. J., 2004, "Sagittal plane biomechanics cannot injure the acl during sidestep cutting," Clinical Biomechanics, **19**(8), pp. 828 – 838.

[5] Gerritsen, K., Van den Bogert, A., Hulliger, M., and Zernicke, R., 1998, "Intrinsic muscle properties facilitate locomotor control - a computer simulation study." Motor Control, **2**, pp. 206–220.

[6] Komura, T., Nagano, A., Leung, H., and Shinagawa, Y., 2005, "Simulating pathological gait using the enhanced linear inverted pendulum model," IEEE Transactions on Biomedical Engineering, **52**(9), pp. 1502–1513.

[7] Goldberg, S. R., Õunpuu, S., and Delp, S. L., 2003, "The importance of swing-phase initial conditions in stiff-knee gait," Journal of Biomechanics, **36**(8), pp. 1111 – 1116.

[8] Piazza, S. J., 2006, "Muscle-driven forward dynamic simulations for the study of normal and pathological gait," Journal of NeuroEngineering and Rehabilitation, **3**(5), pp. 1–7.

[9] Sasaki, K. and Neptune, R. R., 2006, "Muscle mechanical work and elastic energy utilization during walking and running near the preferred gait transition speed," Gait & Posture, **23**(3), pp. 383 – 390.

[10] Sasaki, K. and Neptune, R. R., 2006, "Differences in muscle function during walking and running at the same speed," Journal of Biomechanics, **39**(11), pp. 2005 – 2013.

[11] Yamaguchi, G. and Zajac, F., 1990, "Restoring unassisted natural gait to paraplegics via functional neuromuscular stimulation: a computer simulation study," IEEE Transactions on Biomedical Engineering, **37**(9), pp. 886–902.

[12] Seireg, A. and Arvikar, R., 1989, *Biomechanical Analysis of the Musculoskeletal Structure for Medicine and Sports*, Hemisphere Publishing Corporation, New York, USA.

[13] Crowninshield, R. and Brand, R. A., 1989, "A physiologically based criterion of muscle force prediction in locomotion," Journal of Biomechanics, **14**(11), pp. 793–801.

[14] Happee, R. and der Helm, F. C. T. V., 1995, "The control of shoulder muscles during goal directed movements, an inverse dynamic analysis," Journal of Biomechanics, **28**(10), pp. 1179 – 1191.

[15] Zajac, F., 1989, "Muscle and tendon: properties, models, scaling, and application to biomechanics and motor control," Critical Reviews in Biomedical Engineering, **17**(4), pp. 359–411.

[16] Anderson, F. and Pandy, M., 2001, "Dynamic optimization of human walking," Journal of Biomechanical Engineering, **123**, pp. 381–390.

[17] Lloyd, D. G. and Besier, T. F., 2003, "An EMG-driven musculoskeletal model to estimate muscle forces and knee joint moments in vivo," Journal of Biomechanics, **36**(6), pp. 765 – 776.

[18] Koo, T. K. and Mak, A. F., 2005, "Feasibility of using EMG driven neuromusculoskeletal model for prediction of dynamic movement of the elbow," Journal of Electromyography and Kinesiology, **15**(1), pp. 12–26.

[19] Li, L., Tong, K., Hu, X., Hung, L., and Koo, T., 2009, "Incorporating ultrasound-measured musculotendon parameters to subject-specific EMG-driven model to simulate voluntary elbow flexion for persons after stroke," Clinical Biomechanics, **24**(1), pp. 101–109.

[20] Buchanan, T., Lloyd, D., Manal, K., and Besier, T., 2004, "Neuromusculoskeletal modeling: Estimation of muscle forces and joint moments and movements from measurements of neural command," Journal of Applied Biomechanics, **20**(4), pp. 367–395.

[21] Thelen, D. G., Anderson, F. C., and Delp, S. L., 2003, "Generating dynamic simulations of movement using computed muscle control," Journal of Biomechanics, **36**(3), pp. 321–328.

[22] Thelen, D. G. and Anderson, F. C., 2006, "Using computed muscle control to generate forward dynamic simulations of human walking from experimental data," Journal of Biomechanics, **39**(6), pp. 1107 – 1115.

[23] Seth, A. and Pandy, M., 2007, "A neuromusculoskeletal tracking method for estimating individual muscle forces in human movement," Journal of Biomechanics, **40**(2), pp. 356–366.

[24] Collins, J. J., 1995, "The redundant nature of locomotor optimization laws," Journal of Biomechanics, **28**(3), pp. 251–267.

[25] Cholewicki, J., McGill, S. M., and Norman, R., 1995, "Comparison of muscle forces and joint load from an optimization and EMG assisted lumbar spine model: Towards development of a hybrid approach," Journal of Biomechanics, **28**(3), pp. 321–331.

[26] Jinha, A., Ait-Haddou, R., and Herzog, W., 2006, "Predictions of co-contraction depend critically on degrees-of-freedom in the musculoskeletal model," Journal of Biomechanics, **39**(6), pp. 1145–1152.

[27] Ait-Haddou, R., Binding, P., and Herzog, W., 2000, "Theoretical considerations on cocontraction of sets of agonistic and antagonistic muscles," Journal of Biomechanics, **33**(9), pp. 1105–1111.

[28] Forster, E., Simon, U., Augat, P., and Claes, L., 2004, "Extension of a state-of-the-art optimization criterion to predict co-contraction," Journal of Biomechanics, **37**(4), pp. 577–581.

[29] Baildon, R. and Chapman, A., 1983, "A new approach to the human muscle model," Journal of Biomechanics, **16**(10), pp. 803–809.

[30] Hatze, H., 1981, *Myocybernetic control models of skeletal muscle*, Ph.D. thesis, University of South Africa, Pretoria – South Africa.

[31] Hill, A., 1938, "The heat of shortening and the dynamic constants of muscle," Royal Society of London Proceedings Series B, **126**(843), pp. 136–195.

[32] Riener, R., Quintern, J., and Schmidt, G., 1996, "Biomechanical model of the human knee evaluated by neuromuscular stimulation," Journal of Biomechanics, **29**(9), pp. 1157–1167.

[33] Winter, J. M. and Stack, L., 1985, "Analysis of fundamental human movement patterns through the use of in-depth antagonistic muscle models," IEEE Transactions on Biomedical Engineering, **32**(10), pp. 826–839.

[34] Stroeve, S., 1999, "Impedance characteristics of a neuromusculoskeletal model of the human arm I. posture control," Biological Cybernetics, **81**(5–6), pp. 475–494.

[35] Buchanan, T. S. and Shreeve, D. A., 1996, "An evaluation of optimization techniques for the prediction of muscle activation patterns during isometric tasks," Journal of Biomechanical Engineering, **118**(4), pp. 565–574.

[36] Happee, R., 1994, "Inverse dynamic optimization including muscular dynamics, a new simulation method applied to goal directed movements," Journal of Biomechanics, **27**(7), pp. 953 – 960.

[37] Isidori, A., 1995, *Nonlinear Control Systems*, vol. II of *Communications and Control Engineering Series*, Springer.

[38] Schappacher-Tilp, G., Binding, P., Braverman, E., and Herzog, W., 2009, "Velocity-dependent cost function for the prediction of force sharing among synergistic muscles in a one degree of freedom model," Journal of Biomechanics, **42**(5), pp. 657–660.

[39] Binding, P., Jinha, A., and Herzog, W., 2000, "Analytic analysis of the force sharing among synergistic muscles in one- and two-degree-of-freedom models," Journal of Biomechanics, **33**(11), pp. 1423–1432.

List of Figure Captions

1. Figure 1: Scheme of a musculotendon unit.
2. Figure 2: Hill-type model of a musculotendon unit.
3. Figure 3: The force-length and force-velocity relationships.
4. Figure 4: Contraction dynamics.
5. Figure 5: Minimal normalized musculotendon force.
6. Figure 6: Maximal normalized musculotendon force.
7. Figure 7: Schematic representation of the anthropomorphic arm.
8. Figure 8: Anthropomorphic arm block diagram.
9. Figure 9: The proposed musculoskeletal simulation strategy.
10. Figure 10: Distribution of forces using criterion (21).
11. Figure 11: Distribution of forces using criterion (27).
12. Figure 12: Muscular activations versus time.
13. Figure 13: Elbow position tracking error versus time.

List of Table Captions

1. Table 1: Skeletal parameters of the anthropomorphic arm model.

2. Table 2: Muscle parameters of the arm model.